PERGAMON

International Journal of Heat and Mass Transfer 45 (2002) 4417–4433

International Journal of HEAT and MASS TRANSFER

www.elsevier.com/locate/ijhmt

Effects of flow obstacles on the critical heat flux in a vertical tube cooled with upward flow of R-134a

I.L. Pioro [a,*], D.C. Groeneveld [a,b], S.S. Doerffer [c], Y. Guo [b], S.C. Cheng [b], A. Vasić [b]

[a] *Chalk River Laboratories, AECL, Chalk River, Ont., Canada K0J 1J0*
[b] *Department of Mechanical Engineering, University of Ottawa, Ottawa, Ont., Canada K1N 6N5*
[c] *AECL, Sheridan Park, Mississauga, Ont., Canada L5K 1B2*

Received 15 January 2002; received in revised form 12 April 2002

Abstract

This paper presents a summary of a 4-year investigation into the effect of flow obstacles on critical heat flux (CHF). The investigation was performed using a vertical 6.92 mm tube, cooled with R-134a. The tests covered a pressure range from 0.96 to 2.39 MPa, a mass flux range from 500 to 3000 $kg\,m^{-2}\,s^{-1}$, and an outlet (critical) quality range from −0.05 to +0.95. The following flow obstacle effects on CHF were investigated: (a) the degree of flow blockage (blockage ratios of 12%, 24% and 37%); (b) the flow obstruction shape (cylinder, bar, plate, segment- and sector-shaped obstacles, rings, and twisted plate); (c) the leading and trailing edge shape (abrupt, knife shape, rounded edges); (d) the axial distance separating the flow obstacles, and the distance between the last obstacle and the downstream end of the heated length; (e) the number of obstacles in series; and (f) the location of obstacles within a cross-section.

The test results showed that the presence of flow obstacles generally increases the CHF downstream of the obstacle, although the magnitude of the CHF increase depends on the shape and size of the flow obstacles, the number of obstacles per axial plane, the shape of the leading edge, and their circumferential location, as well as the flow conditions (critical quality, mass flux and pressure).

An improved method for predicting the CHF increase due to the presence of flow obstacles was developed. This semi-analytical method correctly represents the observed parametric and asymptotic trends, including the impact of flow and quality. This method is considered to be a significant improvement over the existing CHF enhancement prediction methods.

Keywords: CHF; Flow boiling; Flow obstacles; Tube; Refrigerant

1. Introduction

Flow obstacles, such as rod spacing devices, have been widely used to maintain the desired cross-sectional configuration in bundle geometries such as nuclear fuel assemblies. Flow obstacles have also been used to enhance critical heat flux (CHF) in tubes and bundle geometries. The effect of obstacles on CHF has been investigated at AECL during the past 20 years [1–5].

During the past four years, the University of Ottawa, in collaboration with AECL, has made an exhaustive study of the effect of flow obstacle characteristics on CHF. Many aspects of this investigation have been reported in previous papers by Pioro et al. [6–9] and Doerffer et al. [1,2], and the details will not be repeated here. The intent of this paper is to present an overview of the findings, including some results that have not yet been reported.

* Corresponding author. Tel.: +1-613-584-8811x4805; fax: +1-613-584-1349.
E-mail address: pioroi@aecl.ca (I.L. Pioro).

0017-9310/02/$ - see front matter
PII: S0017-9310(02)00150-3

Nomenclature

$A_{\text{cr sect}}$	cross-sectional area (mm^2)
a	long side of rectangle (mm)
b	short side of rectangle (mm)
CHF	critical heat flux (kW m^{-2})
CHF_0	critical heat flux without obstacles (kW m^{-2})
D	inside diameter (m)
$G = \rho u$	mass flux ($\text{kg m}^{-2}\,\text{s}^{-1}$)
k_ε	local resistance coefficient
k_{D}	deposition rate (m s^{-1})
L	heated length (m)
L_{SP}	spacer pitch or distance from the obstacle upstream (m)
ℓ	length of obstacle (mm)
P	wetted perimeter (m)
p	pressure (MPa)
R	radius (mm)
u	velocity (m s^{-1})
x	vapor quality
$x_{\text{cr}}^{\text{lim}}$	limiting critical quality

Greek symbols

α	central angle (deg)
δ	thickness (mm)
ε	blockage ratio (flow obstruction cross-sectional area/channel flow area) (%)
μ	coefficient of dynamic viscosity (Pa s)
ρ	density (kg m^{-3})
σ	coefficient of surface tension (N m^{-1})

Subscripts

cr	critical
D	deposition-controlled region
E	entrainment-controlled region
enh	enhanced
f	liquid (referred to fluid at saturation line)
g	vapor (referred to vapor at saturation line)
ID	inside diameter
in	inlet
OD	outside diameter
ref	reference
w	wall

The approach taken in this investigation is to examine the effects of obstacles in a directly heated tube cooled with R-134a. A directly heated tube can be considered as a simulation of a subchannel of a fuel bundle, while R-134a has been found to be an effective modeling fluid that simulates the CHF in water-cooled tubes with and without flow obstacles [1,4]. In all these studies, the impact of flow obstacles on CHF was quantified by the ratio of *CHF of an obstacle-equipped test section/CHF for a reference test section without obstacles* for the same local flow conditions (pressure, mass flux, and critical quality (i.e., quality at dryout)). This ratio will also be referred to as the enhancement ratio K.

2. Experiments

The experimental study was performed in the University of Ottawa multi-fluid loop, using R-134a as a coolant (Fig. 1) [6–9]. The test section was a vertical tube (ID 6.92 mm, OD 7.93 mm, length 2.1 m), made of Inconel 601 (Fig. 2). The test section was directly heated by DC current flowing through the wall. Many types of flow obstacles (see Figs. 2–5 and Tables 1–3) were used: local flow obstacles and concentric rings. The axial length (in the direction of the flow) of the blockages was usually 10 mm (except for ring-shaped obstacles, which were 3 mm in length) and the blockage ratio ε was 12%, 24% or 37%. In most tests, 10 rings, each with a blockage ratio of 37% were spaced evenly at a distance of 125 mm upstream of the main flow obstacle(s) to prevent premature dryout upstream of main flow obstacle(s) (Fig. 2). Previous studies conducted at the University of Ottawa did not reveal a cumulative effect of flow obstacles on CHF [6,7,9]. The local flow obstacle(s) and the rings were kept in their locations with external magnets.

Most of the tests were performed at an outlet pressure of 1.67 MPa (10 MPa in water-equivalent value). Additional tests were performed at outlet pressures of 0.96, 1.31, 2.03, and 2.39 MPa. The range of inlet temperature (2–56 °C) was as wide as possible, but was limited by the temperature of the water in the condenser and the saturation temperature. This range corresponded to a maximum inlet quality range of −60% to −2%. To increase range of critical qualities, different heated lengths were used. The heated length was changed by moving the upstream power clamp towards the downstream end of the tube. Additional tests were performed with two-phase flow at the test section inlet. This allowed the effect of obstacles within an even wider range of critical qualities to be investigated. Previous studies at the University of Ottawa did not reveal a noticeable effect of various heated lengths and two-phase flow at the test section inlet on CHF [6–11]. The complete test matrix and their water-equivalent values are listed in Table 4.

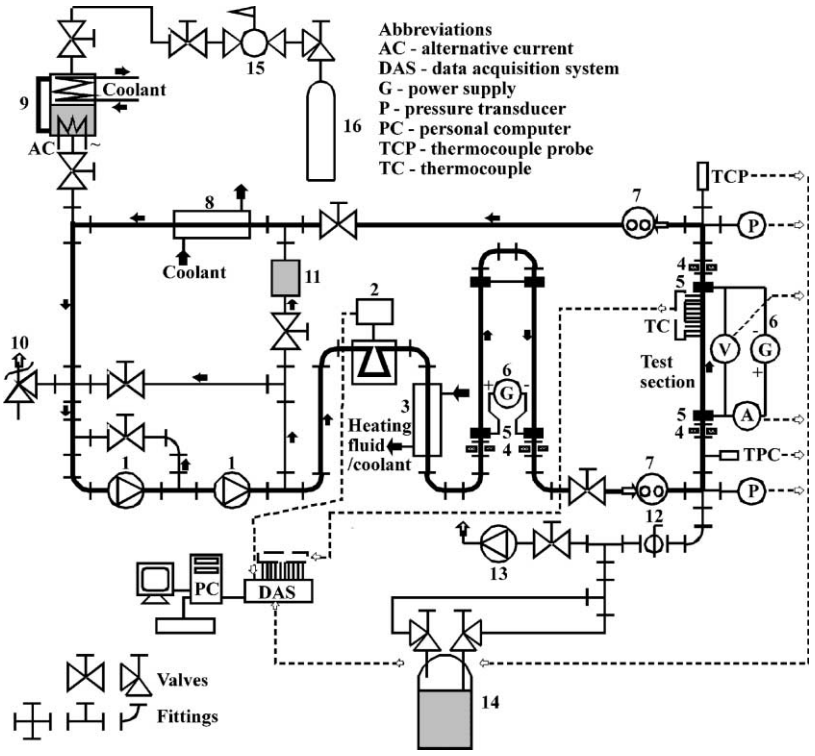

Fig. 1. Experimental multi-fluid loop: 1—gear pump, 2—Coriolis type flowmeter, 3—preheater, 4—dielectric fittings, 5—power terminals, 6—electrical preheater, 7—sight glass, 8—condenser, 9—pressurizer, 10—pressure relief valve, 11—refrigerant filter-dryer, 12—ball valve, 13—vacuum pump, 14—refrigerant storage tank, 15—pressure transducer, 16—nitrogen container.

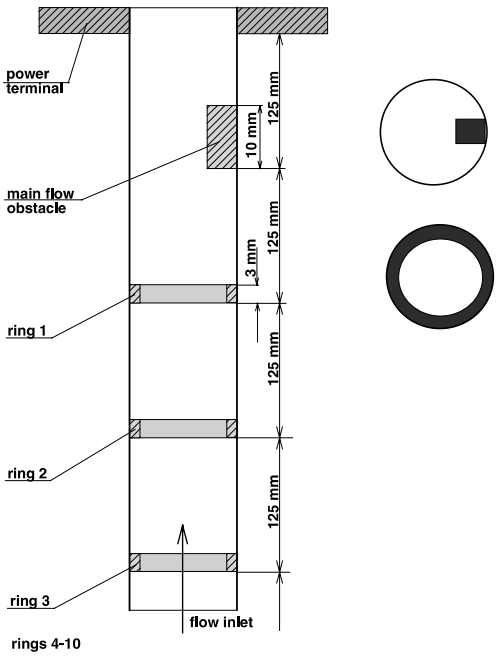

Fig. 2. Test section—CHF enhanced tube (ID 6.92 mm).

3. Test results

3.1. General

The CHF test results obtained in the enhanced tube [1] were compared with the corresponding reference CHF values in the reference tube [2] at the same flow, pressure and critical quality. The reference tube results were obtained from two sources: (i) reference tube tests obtained using R-134a from the University of Ottawa experimental loop [10,11], and (ii) the CHF look-up table for water [12]. The CHF look-up table for water was converted into R-134a-equivalent data using fluid-to-fluid modeling relationships, as described by Groeneveld et al. [4], and the converted values were compared with the reference tube data [11,13]. In general, the agreement between the CHF look-up table [12] and the experimental data is good beyond the limiting critical quality region [11]. At qualities near the so-called *limiting*

[1] Tube equipped with flow obstacles.
[2] Tube without flow obstacles (bare tube).

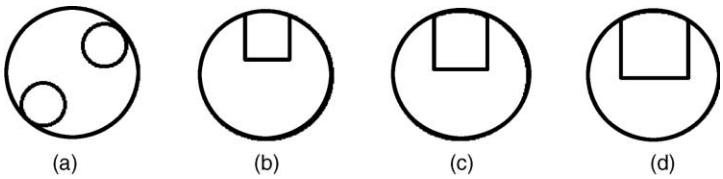

Fig. 3. Cross-sectional shape of flow obstructions: (a) two cylinders 180° apart ($\varepsilon = 12\%$ each); (b) square bar with one rounded side ($\varepsilon = 12\%$); (c) the same ($\varepsilon = 24\%$); (d) the same ($\varepsilon = 37\%$).

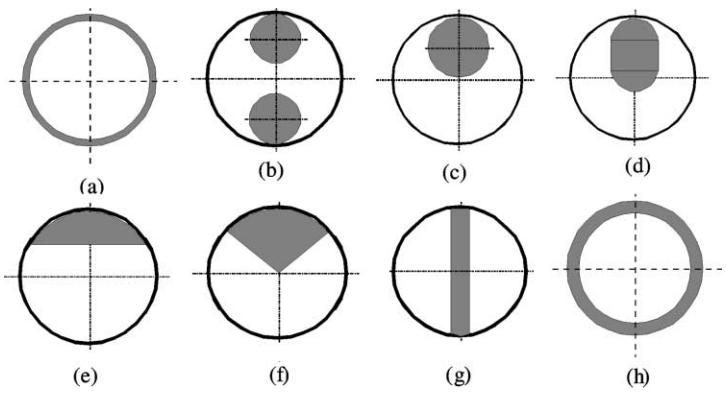

Fig. 4. Various cross-sectional shapes of flow obstructions: (a) ring ($\varepsilon = 24\%$); (b) two cylinders 180° apart ($\varepsilon = 12\%$ each); (c) cylinder ($\varepsilon = 24\%$); (d) bar with two rounded sides ($\varepsilon = 24\%$); (e) segment ($\varepsilon = 24\%$); (f) sector ($\varepsilon = 24\%$); (g) plate ($\varepsilon = 24\%$); (h) ring ($\varepsilon = 37\%$).

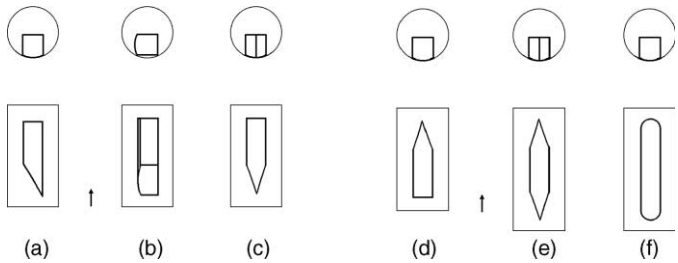

Fig. 5. Flow obstructions—square bars (one side rounded, $\varepsilon = 24\%$) with various edges: (a) wedge-shaped leading edge directed to side; (b) the same, directed to center; (c) knife-shaped leading edge; (d) knife-shaped trailing edge; (e) knife-shaped both edges; (f) rounded both edges.

Table 1
Obstacles specification (see Fig. 3)

Figure	Type of obstacle and blockage ratio	Length (mm)	Width (mm)	Height (mm)	Diameter (OD)/mm
Cylindrical obstacles					
Fig. 3a	Two cylinders, 12% each	10	–	–	2.4
Square bars with one rounded side ($R_{\text{rounded side}} = 3.46$ mm)					
Fig. 3b	Square bar, 12%	10	2.1	2.26	–
Fig. 3c	Square bar, 24%	10	2.9	3.22	–
Fig. 3d	Square bar, 37%	10	3.5	3.98	–

Table 2
Dimensions of test section and flow obstructions (see Fig. 4)

	ε (%)	D (mm)	D_{OD} (mm)	$\delta_w(\delta)$ (mm)	ℓ (mm)	$A_{cr\,sect}$ (mm^2)	
						Flow	Obstruction
Test section							
Tube	–	6.92	7.94	0.51	–	37.6	–
Flow obstructions							
Ring (Fig. 4a)	24	6.05	6.92	0.44	3	28.7	8.86
Cylinder (Fig. 4b)	12	–	2.36	–	10	–	4.4
Cylinder (Fig. 4c)	24	–	3.34	–	10	–	8.8
Bar (Fig. 4d)	24	–	$R_{round} = 1.95$	(2.36)	10	–	8.6
Segment (Fig. 4e)	24	–	$R_{arc} = 3.46$	(2)	10	–	9.05
Sector (Fig. 4f)	24	–	$R_{arc} = 3.46$	$\alpha = 86°$	10	–	9.05
Plate (Fig. 4g)	24	–	$a = 6.78$	$b = 1.4$	10	–	9.49
Ring (Fig. 4h)	37	5.5	6.92	0.71	3	23.8	13.8
Twisted plate	24	–	$a = 6.78$	$b = 1.4$	19	–	9.49
Ring	29	5.22	6.43	0.6	3	26.5	11.1

Table 3
Obstacles specification (see Fig. 5)

Figure	Type of obstacle and blockage ratio (%)	Length (mm)	Width (mm)	Height (mm)
Square bars with one rounded side $R_{rounded\ side} = 3.46$ mm)				
Fig. 5a and b	Wedged-shaped edge, 24%	15	2.9	3.22
Fig. 5c and d	Knife-shaped edge, 24%	15	2.9	3.22
Fig. 5e	Knife-shaped both edges, 24%	20	2.9	3.22
Fig. 5f	Rounded both edges, 24%	20	2.9	3.22

Table 4
Test conditions for reference tube and CHF enhanced tube

Flow parameters	Reference/enhanced tube	Water-equivalent value
Pressure	0.96 MPa	6 MPa
	1.31 MPa	8 MPa
	1.67 MPa	10 MPa
	2.03 MPa	12 MPa
	2.39 MPa	14 MPa
Inlet quality	−60% to −2%	Same
Mass flux ($p = 0.96$ MPa)	2000 kg m^{-2} s^{-1}	2855 kg m^{-2} s^{-1}
	3000 kg m^{-2} s^{-1}	4282 kg m^{-2} s^{-1}
Mass flux ($p = 1.31$ MPa)	2000 kg m^{-2} s^{-1}	2846 kg m^{-2} s^{-1}
	3000 kg m^{-2} s^{-1}	4269 kg m^{-2} s^{-1}
Mass flux ($p = 1.67$ MPa)	500 kg m^{-2} s^{-1}	707 kg m^{-2} s^{-1}
	1000 kg m^{-2} s^{-1}	1413 kg m^{-2} s^{-1}
	2000 kg m^{-2} s^{-1}	2826 kg m^{-2} s^{-1}
	3000 kg m^{-2} s^{-1}	4239 kg m^{-2} s^{-1}
Mass flux ($p = 2.03$ MPa)	2000 kg m^{-2} s^{-1}	2796 kg m^{-2} s^{-1}
	3000 kg m^{-2} s^{-1}	4194 kg m^{-2} s^{-1}
Mass flux ($p = 2.39$ MPa)	2000 kg m^{-2} s^{-1}	2806 kg m^{-2} s^{-1}
	3000 kg m^{-2} s^{-1}	4209 kg m^{-2} s^{-1}
Outlet quality	−5 to +95%	Same
Heated length	0.45–2 m	Same

critical quality region (i.e., the region where the CHF drops very rapidly with increasing inlet quality, due to a transition from entrainment-controlled dryout to deposition-controlled dryout), a different trend can be seen;

here, the CHF look-up table shows a more gradual variation in CHF. The CHF look-up table extends over a much wider range of qualities than the experiments. This permits us to quantify the CHF enhancement for qualities greater than the investigated range of the reference tube.

3.2. Effect of flow conditions on CHF enhancement

In Fig. 6, the variation of CHF vs. x_{cr} for the reference tube and for the CHF-enhanced tube equipped with two cylindrical obstacles ($\varepsilon = 12\%$ for each, and they are located 180° apart in one cross-sectional plane, as shown in Fig. 3a, along with 10 upstream rings (Fig. 2), each having $\varepsilon = 37\%$) is compared at various mass fluxes ($G = 500$, 1000, 2000 and 3000 $\mathrm{kg\,m^{-2}\,s^{-1}}$) and $p = 1.67$ MPa. Fig. 7a summarizes these results by plotting the CHF enhancement ratio against x_{cr} for all flows (i.e., for 500, 1000, 2000, and 3000 $\mathrm{kg\,m^{-2}\,s^{-1}}$). Similar trends were also obtained with different flow obstacles, details of the flow obstacle shape effect will be discussed in Section 3.5. Based on these results, it may be concluded that

1. Flow obstacles remove the steep reduction in the CHF vs. x_{cr} curve within limiting critical quality region, by increasing the CHF in the deposition-controlled region. Since flow obstacles increase the turbulence level, they will also increase the deposition rate. This impact on the deposition rate is most important in the deposition-controlled region (beyond the limiting critical quality region), where the CHF is particularly low for low flow conditions (Fig. 6a and b).
2. For the pre-limiting critical quality region, flow obstacles have a relatively small effect on CHF at low flows, and could even reduce the CHF. This trend is shown very clearly in Fig. 7a, and also by comparing Fig. 6a and b with c and d, respectively. This trend is thought to be due to a possible negative effect of obstacles on entrainment at lower flows, where the interference of the obstacles with the liquid film could

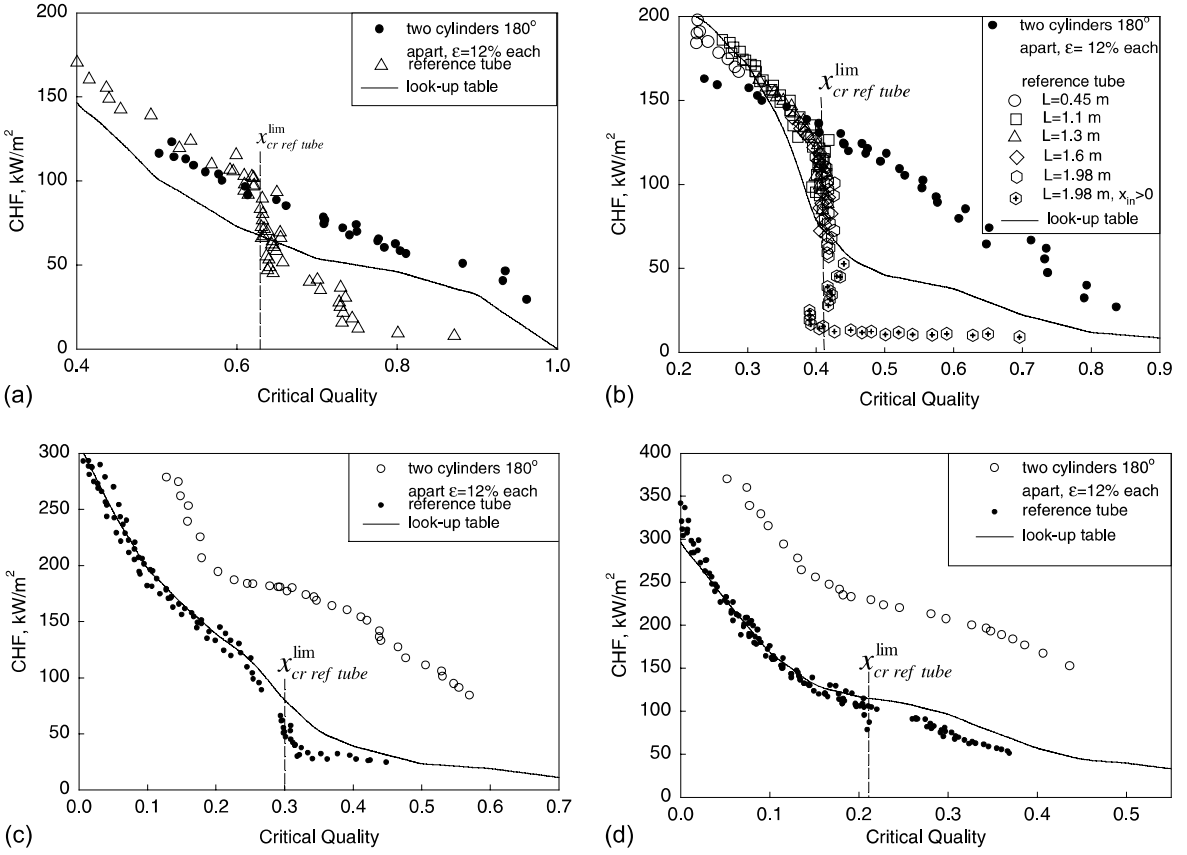

Fig. 6. Effect of critical quality on CHF in reference and enhanced tubes: R-134a, $p = 1.67$ MPa, $L = 0.45$–2 m, flow obstructions pitch 125 mm: (a) $G = 500$ $\mathrm{kg\,m^{-2}\,s^{-1}}$, (b) $G = 1000$ $\mathrm{kg\,m^{-2}\,s^{-1}}$, (c) $G = 2000$ $\mathrm{kg\,m^{-2}\,s^{-1}}$, (d) $G = 3000$ $\mathrm{kg\,m^{-2}\,s^{-1}}$.

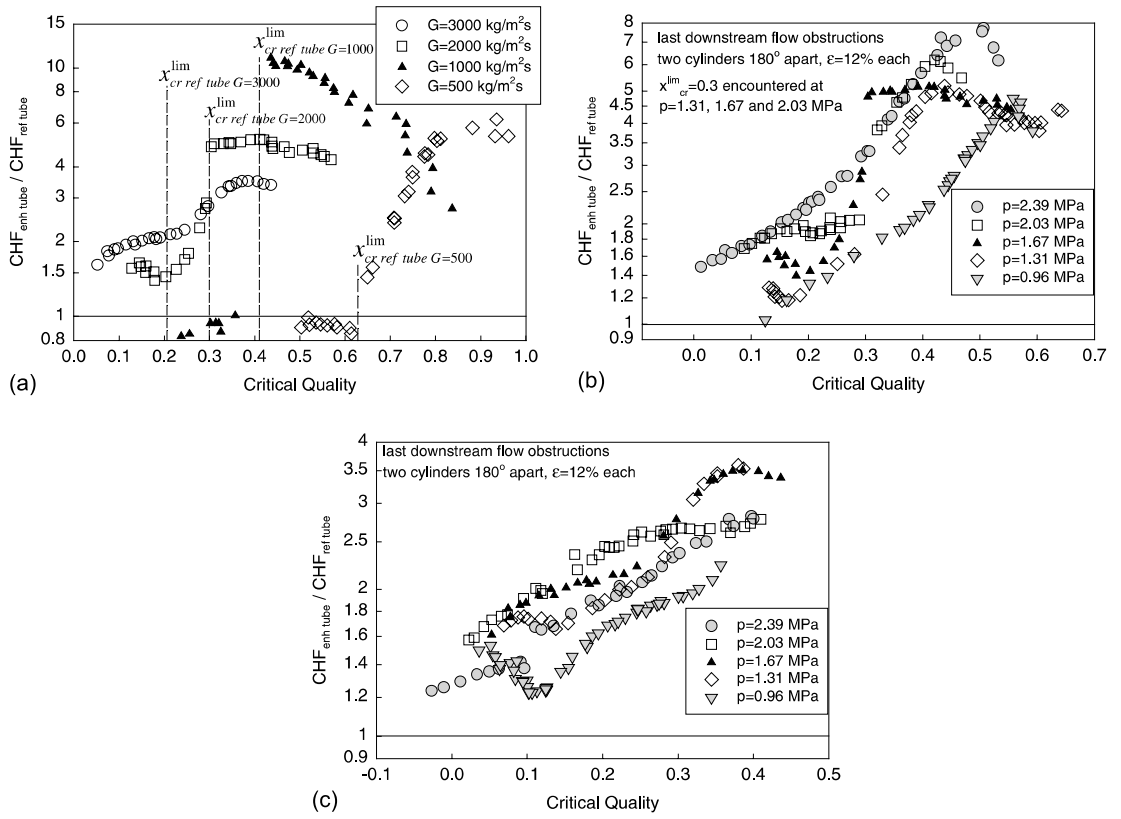

Fig. 7. Effect of critical quality on CHF enhancement in enhanced tube (last downstream flow obstructions—two cylindrical obstacles 180° apart, $\varepsilon = 12\%$ each): R-134a, $L = 0.45$–2 m, flow obstructions pitch 125 mm: (a) at different mass fluxes, $p = 1.67$ MPa, (b) at different pressures, $G = 2000\ \mathrm{kg\,m^{-2}\,s^{-1}}$, (c) at different pressures, $G = 3000\ \mathrm{kg\,m^{-2}\,s^{-1}}$.

increase the entrainment rate. For higher flows, obstacles increase the CHF at all qualities (Fig. 6c and d).

The effect of pressure on CHF enhancement, although noticeable, is less dramatic compared to the mass flux and critical quality effect. Fig. 7b and c shows the effect of pressure ($p = 0.96$, 1.31, 1.67, 2.03, and 2.39 MPa) on CHF enhancement for two cylindrical obstacles ($\varepsilon = 12\%$ for each) located 180° apart in one cross-sectional plane, along with 10 upstream rings (each having $\varepsilon = 37\%$), and at two values of mass flux ($G = 2000$ and $3000\ \mathrm{kg\,m^{-2}\,s^{-1}}$). The effect of pressure on CHF enhancement was not investigated at the lower mass fluxes.

3.3. Effect of blockage-ratio on CHF

Experiments in the enhanced tube were initially performed with one plane containing the main local obstacle(s), either a single bar obstacle, with $\varepsilon = 12\%$, 24%, or 37%, as shown in Fig. 3b–d, or two bars, located 180° apart in one cross-sectional plane, with $\varepsilon = 12\%$ for each located 125 mm upstream from the upper power terminal. Ten additional ring-shaped flow obstacles (each having $\varepsilon = 37\%$) were located upstream of the local obstacle(s) and were spaced 125 mm from each other, as shown schematically in Fig. 2.

Fig. 8a–c shows the CHF results for mass flux values of 2000 and $3000\ \mathrm{kg\,m^{-2}\,s^{-1}}$. It is clear that the flow blockage ratio has a strong effect on CHF; the local flow obstacles with the largest blockage ratio show the highest increase in CHF (Fig. 8d). For qualities higher than the limiting critical quality for the reference tube, this increase is dramatic (up to 12 times, see Fig. 7a).

3.4. Effect of axial distance between obstacles

In a parallel experiment, Doerffer et al. [2] investigated the effect of axial pitch on CHF under similar conditions, and found that the CHF enhancement decays exponentially with an increase in axial pitch between adjacent obstacles. Fig. 9 provides further confirmation of Doerffer's observation. This figure shows the effect of the distance from the upper power terminal to the last downstream ring on CHF enhancement, for a tube with

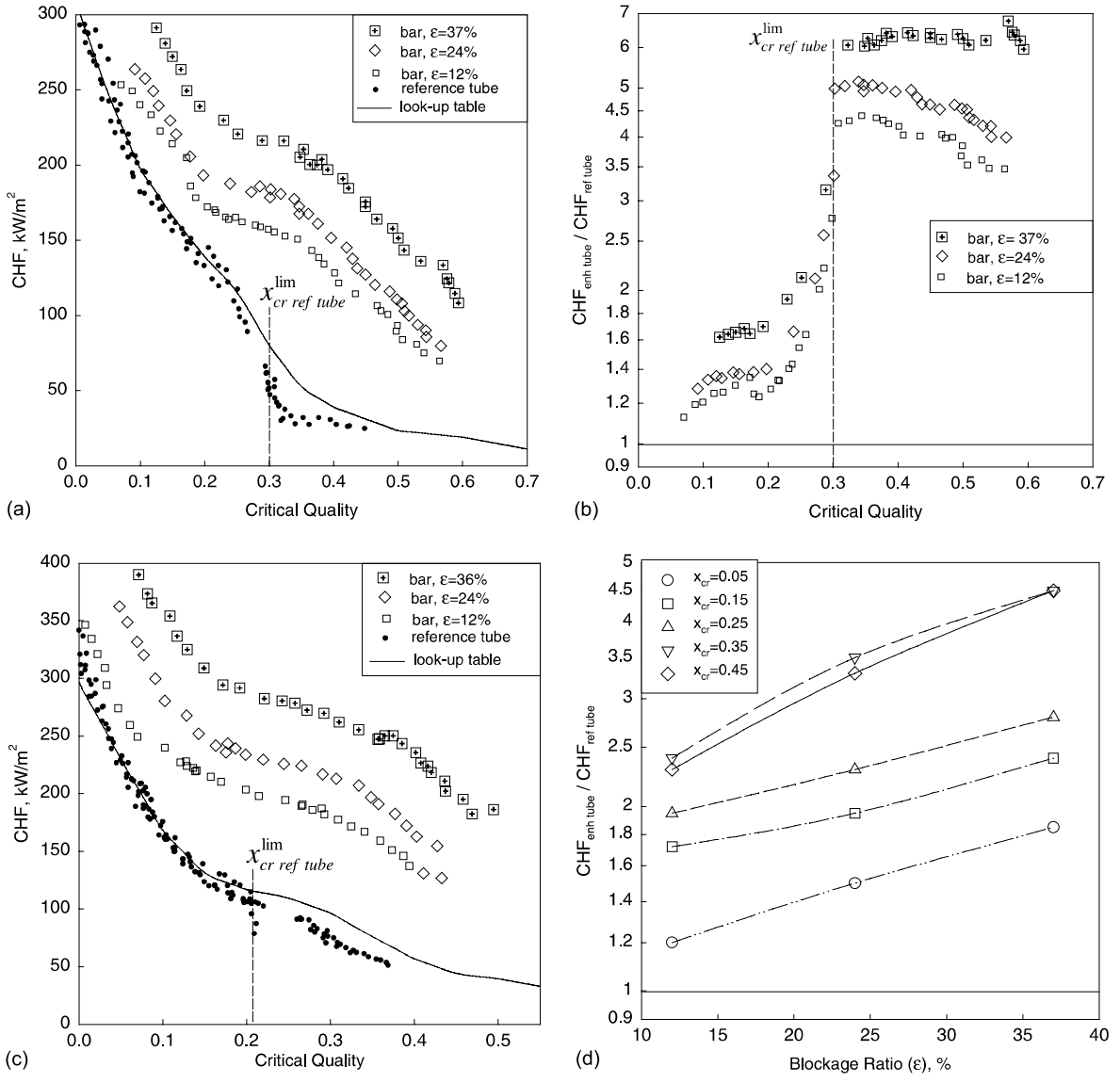

Fig. 8. Effect of critical quality on CHF in reference and enhanced tubes (a, c) and on CHF enhancement in enhanced tube (b) and effect of blockage ratio on CHF enhancement in enhanced tube (d): R-134a, $p = 1.67$ MPa, $L = 0.45$–2 m, flow obstructions pitch 125 mm; (a, b) $G = 2000\ \mathrm{kg\,m^{-2}\,s^{-1}}$, (c) $G = 3000\ \mathrm{kg\,m^{-2}\,s^{-1}}$, (d) last downstream flow obstruction—bar, $G = 3000\ \mathrm{kg\,m^{-2}\,s^{-1}}$.

10 rings (each having $\varepsilon = 37\%$) at $G = 3000\ \mathrm{kg\,m^{-2}\,s^{-1}}$. The distance between the upstream rings was not varied in this experiment; however, as was shown by Doerffer [14], the effect of the upstream rings would not have been significant, as it is primarily the distance from the nearest upstream obstacle that determines the CHF enhancement effect. In general, the axial distance effect on CHF enhancement is very significant (Fig. 9b and c). The CHF enhancement decays exponentially with increasing distance from the nearest upstream flow blockage. Similar results were also observed for $G = 2000$ and 1000 $\mathrm{kg\,m^{-2}\,s^{-1}}$.

3.5. Effect of flow obstruction shape on CHF

This part of the study covered a wide range of flow obstacle shapes, shown in Fig. 4: twister (19-mm-long plate twisted about 90°), sector, segment, bar, cylinder, two small cylinders, bar, two small bars, ring, and plate (see also Table 2 for more details). All of these obstacles had the same flow blockage ratio of 24%, and they all were installed 125 mm upstream from the downstream heated end [7]. The results were compared to the reference tube CHF measurements and the CHF look-up table, as shown in Figs. 10 and 11, where the CHF is

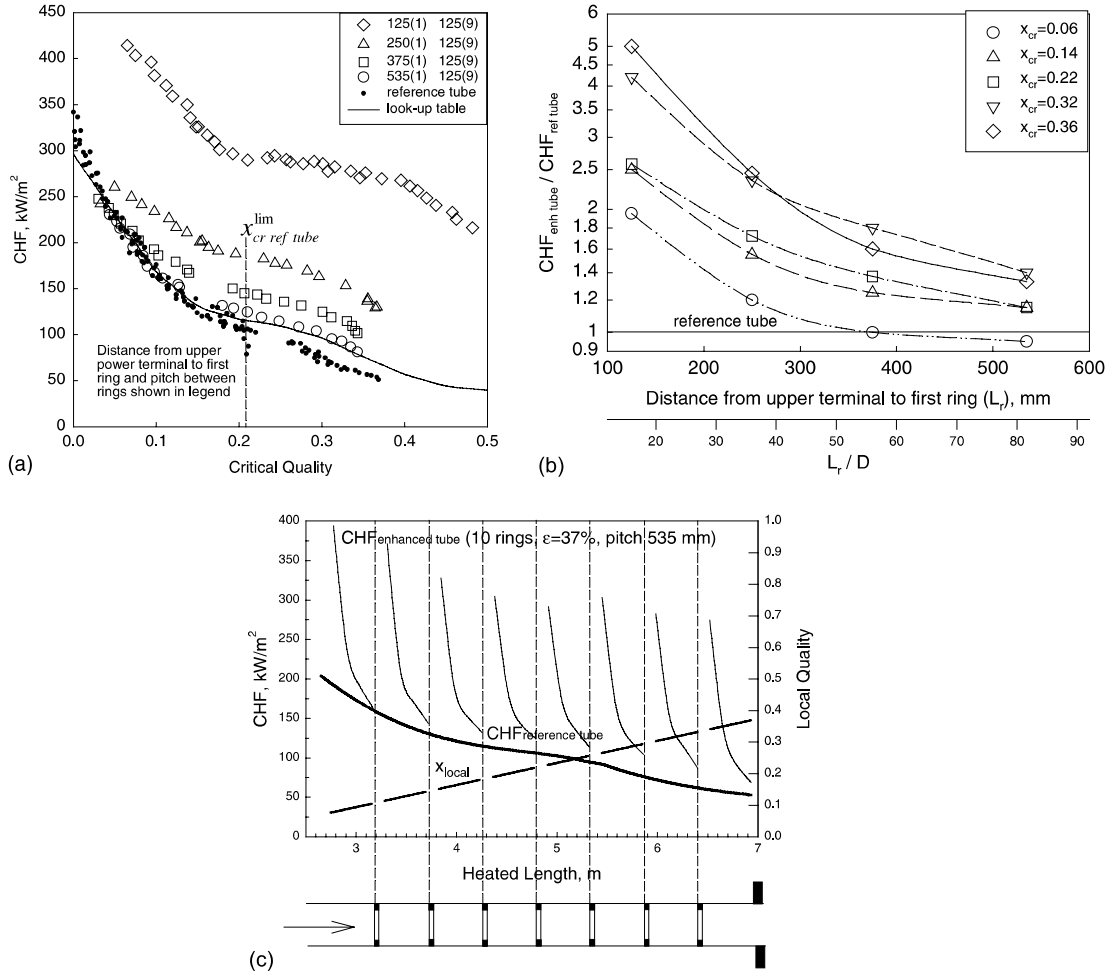

Fig. 9. Effect of critical quality on CHF in reference and enhanced tubes (a), effect of distance from downstream power terminal to first ring on CHF enhancement in enhanced tube (b) and effect of heated length on CHF enhancement in vertical enhanced tube (calculated values based on experimental data) (c): R-134a, $p = 1.67$ MPa, $G = 3000\ \mathrm{kg\,m^{-2}\,s^{-1}}$, $D = 6.92$ mm, flow obstructions—10 rings, $\varepsilon = 37\%$; (a) $L = 0.45$–2 m, (b) $L = 0.45$–2 m, pitch 125 mm, (c) $L = 6.93$ m (single-phase flow at inlet; equivalent-heated length re-calculated based on experimental data for two-phase flow at inlet).

plotted against x_{cr} for $G = 2000$ and $3000\ \mathrm{kg\,m^{-2}\,s^{-1}}$, respectively. Figs. 10b and 11b show the ratio $\mathrm{CHF_{enh\ tube}}/\mathrm{CHF_{ref\ tube}}$.

Most of the obstacles have a similar enhancement effect on the CHF. The effect of flow conditions on CHF enhancement were also similar and were discussed in Section 3.2. The various shapes do not provide identical CHF enhancement:

(1) At $G \leqslant 2000\ \mathrm{kg\,m^{-2}\,s^{-1}}$ and $x_{cr} < x_{cr}^{lim}$, the ring appeared to be least effective. This is expected, since ring-shaped obstacles provide more interference with the liquid film, thus resulting in stronger entrainment and a larger detrimental effect on CHF in the entrainment-controlled region. At the highest flow (Fig. 11a), where the demarcation between entrainment-controlled and deposition-controlled regions becomes blurred, the ring CHF enhancement effect becomes similar to that of the other shapes. These results should not be extrapolated to lower mass fluxes.

(2) Tests performed with the plate twisted 90° (thus resembling a very short twisted tape) gave very different results. As expected, the centrifugal effect provided an additional increase in the droplet deposition rate, thus increasing the CHF. Fig. 10a shows that the CHF enhancement using twisted plate was superior to any of the other flow obstacles that were tested. Although the twisted tapes are ideal for round tubes, they cannot be used in bundle subchannels.

(3) Fig. 11c and d shows the comparison between CHF values for one bar vs. two bars located 180° apart in

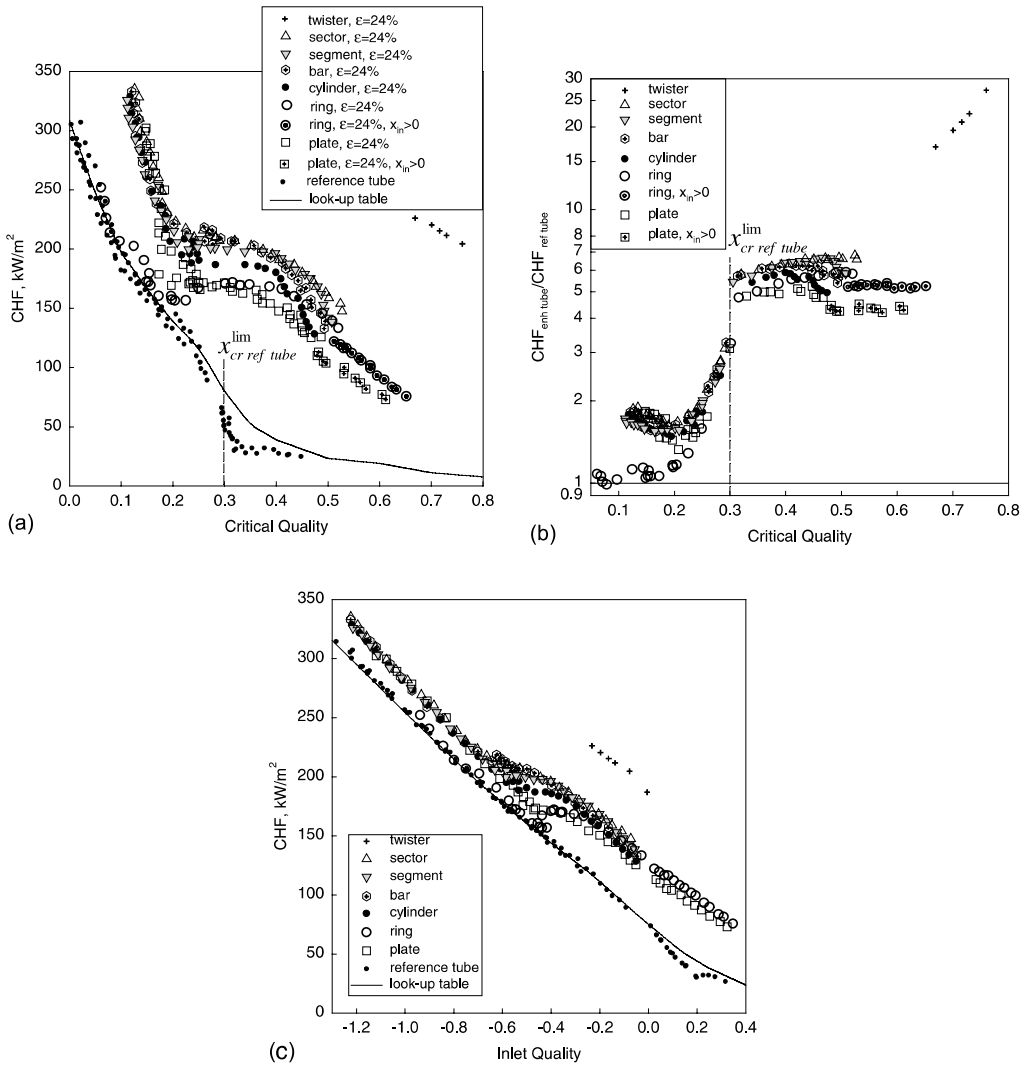

Fig. 10. Effect of quality on CHF in reference and enhanced tubes (a, c) and on CHF enhancement in enhanced tube (b): R-134a, $p = 1.67$ MPa, $G = 2000\ \mathrm{kg\,m^{-2}\,s^{-1}}$; (a, b) effect of critical quality, $L = 0.45$–2 m, (c) effect of inlet quality, $L = 1.98$ m (x_{in} for all heated lengths converted to equivalent-heated length [11,13] of 1.98 m).

one cross-sectional plane. In general, there appears to be no significant effect on enhancement, as long as the total flow blockage is 24%. Additional tests were performed with cylinders instead of bars, which showed very similar results.

3.6. Effect of shape of the leading and trailing edge of the flow obstacles on CHF

The effect of changes in the leading and/or trailing edges of flow obstacles, as shown in Fig. 5, was also investigated [9]. In Fig. 12a and b, the CHF enhancement for the bar with abrupt edges is compared to that for the same cross-sectional-shaped obstacle with knife-shaped leading and/or trailing edges, at mass flux values of 2000 and 3000 $\mathrm{kg\,m^{-2}\,s^{-1}}$. The figures clearly show that the local flow obstacles with abrupt edges show the highest increases in CHF (Fig. 12a and b). When the leading edge is changed to a knife-edge shape, the CHF is lowered; however, an increase in CHF is still provided, especially at the higher critical qualities. The shape of the trailing edge does not appear to have any significant effect on CHF enhancement.

Fig. 12c shows the effect on CHF of differently shaped leading edges (knife-shaped, or wedge-shaped edge directed to the side or the center) of a local flow obstruction (bar, $\varepsilon = 24\%$) at $G = 2000\ \mathrm{kg\,m^{-2}\,s^{-1}}$. The wedge-shaped leading edge that directs the near-wall liquid to

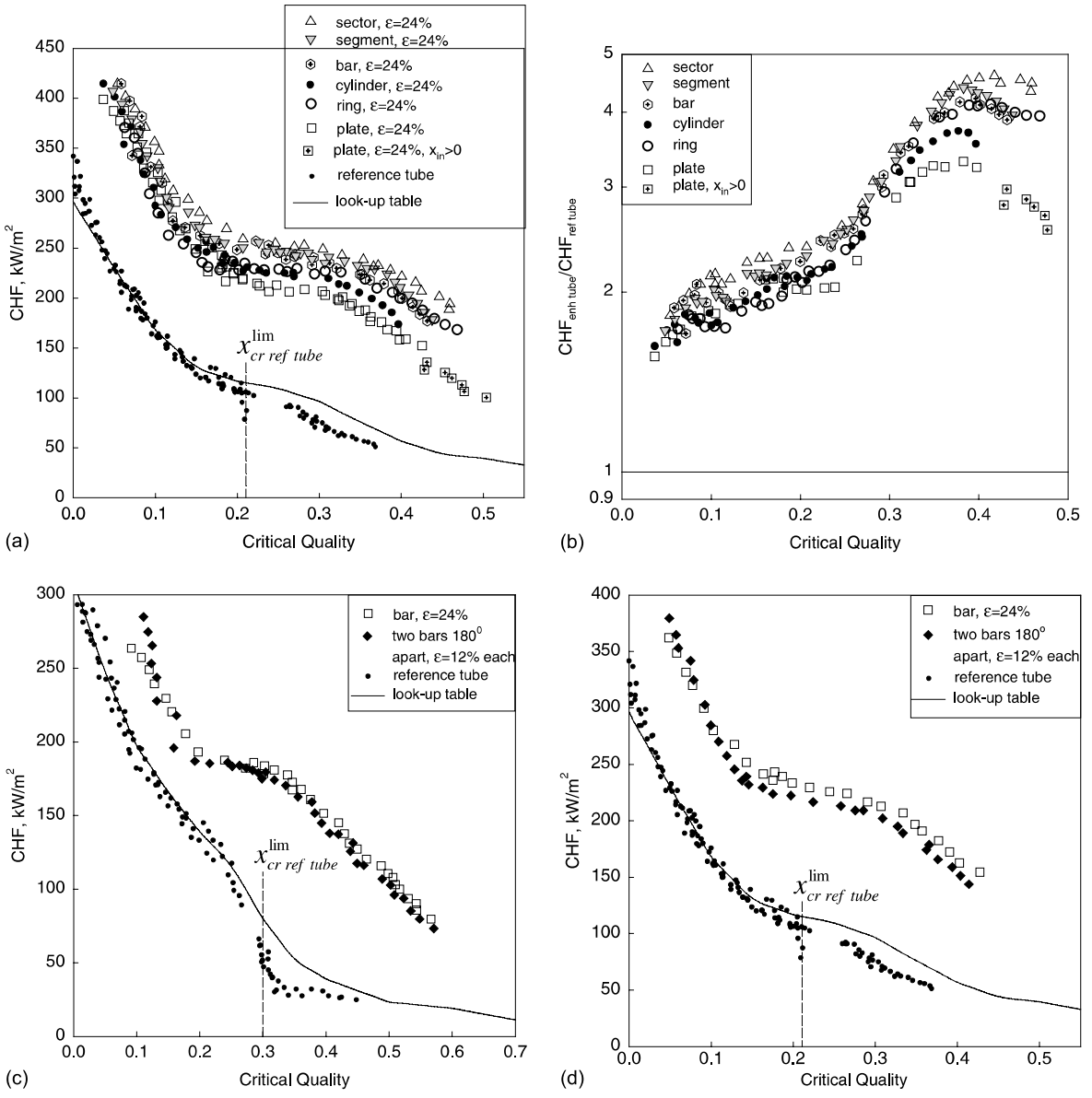

Fig. 11. Effect of critical quality on CHF in reference and enhanced tubes (a, c, d) and on CHF enhancement in enhanced tube (b): R-134a, $p = 1.67$ MPa, $L = 0.45$–2 m, pitch 125 mm; (a, b) $G = 3000\ \mathrm{kg\,m^{-2}\,s^{-1}}$, (c) $G = 2000\ \mathrm{kg\,m^{-2}\,s^{-1}}$, (d) $G = 3000\ \mathrm{kg\,m^{-2}\,s^{-1}}$.

the center of the tube shows slightly less enhancement than the other two shapes. Similar results were obtained at $G = 3000\ \mathrm{kg\,m^{-2}\,s^{-1}}$. At the lower value of mass flux ($G = 2000\ \mathrm{kg\,m^{-2}\,s^{-1}}$), a wedge-shaped leading edge directed to the side shows a higher CHF enhancement than the other two shapes at higher qualities (Fig. 12c).

3.7. Effect of circumferential location of flow obstacles

Fig. 13a and b shows the effect of the circumferential location of flow obstacles. No strong effect due to circumferential location was observed, which supports the previous observation that the total flow blockage in a cross-section is the most important parameter. A minor increase in CHF appears to be present for two cylindrical obstacles located 120° apart.

3.8. Effect of axial offset on CHF

The effect of axial offset refers to a small axial offset of two obstacles that are nominally located in the same cross-sectional plane. Fig. 13c and d shows the effect of

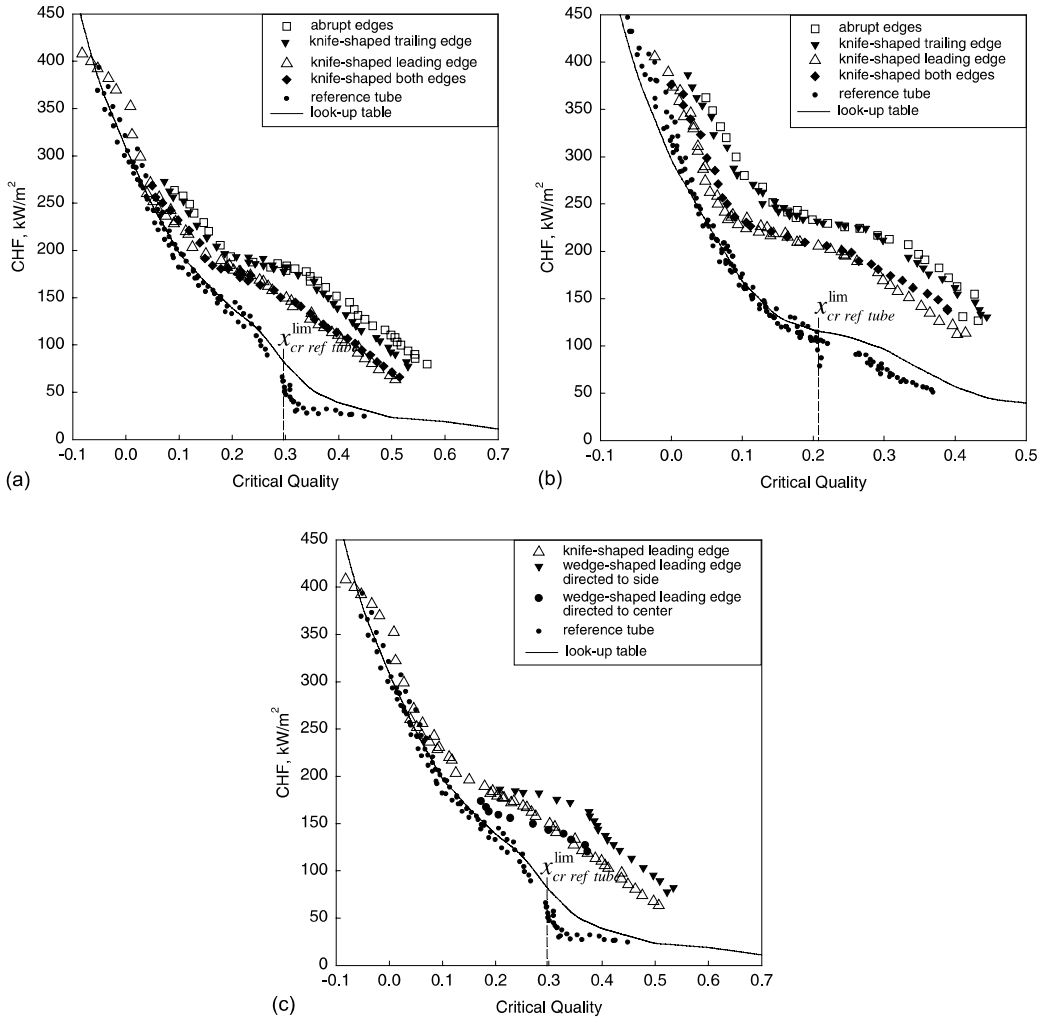

Fig. 12. Effect of critical quality on CHF in reference and enhanced tubes: R-134a, $p = 1.67$ MPa, $L = 0.45$–2 m, $\varepsilon = 24\%$ for last downstream flow obstruction (various leading and trailing edges (a) and (b), various leading edges (c)), pitch 125 mm, (a) $G = 2000$ kg m^{-2} s^{-1}, (b) $G = 3000$ kg m^{-2} s^{-1}, (c) $G = 2000$ kg m^{-2} s^{-1}.

an axial offset of two flow obstacles on CHF. The effect of the offset is minimal, with a slightly lower CHF than the zero axial offset case being observed at lower qualities.

3.9. Detrimental effects of flow obstacles

Fig. 14 clearly shows that at some flow conditions (usually at a mass flux of 1000 kg m^{-2} s^{-1} or less), and at qualities less than the limiting critical quality range for the reference tube), the CHF values in the enhanced tube can be less than those in the reference tube. This result applies to various blockage ratios and configurations of flow obstacles.

Fig. 15 shows that, at some flow conditions and for flow obstacles attached to the wall with abrupt edges (cylinders, rings, etc.), CHF can occur first just upstream of flow obstacles. A more detailed analysis shows that these CHF values at dryout are the same as those in the reference tube, i.e., there is no CHF enhancement just upstream of flow obstacles, although there is also no detrimental effect on CHF.

The mechanism of drypatch spreading along the enhanced and reference tubes is not the same. In general, the dryouts in the enhanced tube "jump" from the downstream end to upstream of the flow obstacles. In a reference tube, the drypatch spreads gradually upstream from the downstream end, with increasing power.

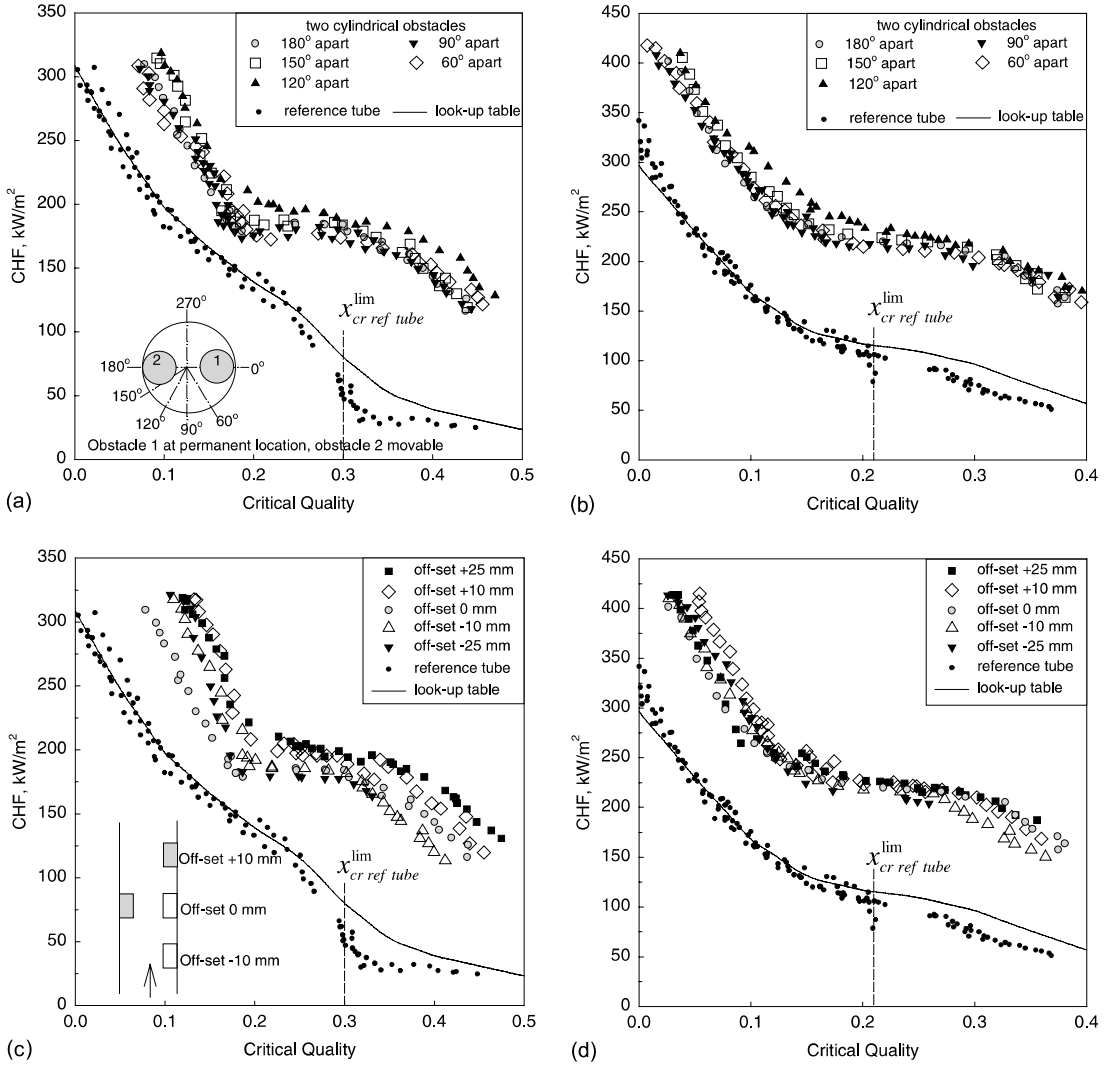

Fig. 13. Effect of critical quality on CHF in reference and enhanced tubes at various circumferential (a, b) and off-set (c, d) locations of obstacles: R-134a, $p = 1.67$ MPa, $L = 0.45$–2 m, last downstream flow obstructions—two cylindrical obstacles, $\varepsilon = 12\%$ each, pitch 125 mm; (a, c) $G = 2000\ \mathrm{kg\,m^{-2}\,s^{-1}}$, (b, d) $G = 3000\ \mathrm{kg\,m^{-2}\,s^{-1}}$.

4. Improved prediction method

4.1. Dominant CHF mechanisms

At low flow qualities, the flow regime is either bubbly flow or annular flow, with a thick liquid film on the wall. CHF occurs in these regimes because of an inadequate removal of bubbles from the wall (departure from nucleate boiling (DNB)-type dryout) and/or a depletion of the liquid film on the wall (entrainment-controlled film dryout). The CHF vs. x_{cr} curve in this region is smooth; hence, there is a gradual change in the CHF mechanism between DNB- and entrainment-controlled dryout. At higher flow qualities, the flow regime is also annular flow, but the liquid film is very thin and the primary supply of liquid to the film is through deposition from the entrained droplets in the core region (deposition-controlled dryout). The changeover to deposition-controlled dryout takes place in the limiting quality region, where the CHF drops sharply, compared to the smooth decline in CHF with critical quality elsewhere.

4.2. Proposed correlation

The experimental results have shown that, in both quality regions, the CHF enhancement ratio follows the generally accepted exponential decaying function:

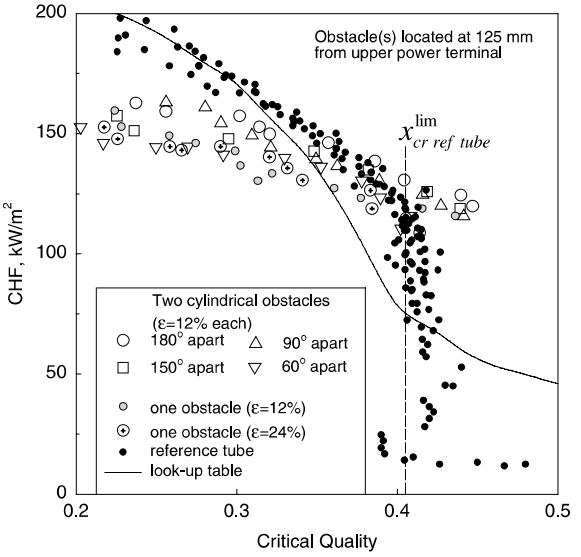

Fig. 14. Effect of critical quality on CHF in reference and enhanced tubes: R-134a, $p = 1.67$ MPa, $G = 1000$ kg m^{-2} s^{-1}, $L = 0.45$–2 m, additional obstructions—3 rings ($\varepsilon = 29\%$), pitch 100 mm.

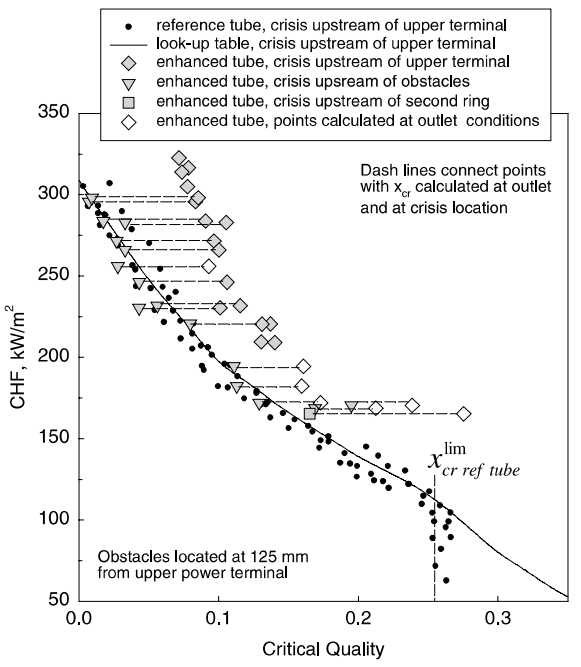

Fig. 15. Effect of critical quality on CHF in reference and enhanced tubes: R-134a, $p = 1.67$ MPa, $G = 2000$ kg m^{-2} s^{-1}, $L = 0.45$–2 m, two cylindrical obstacles (180° apart, $\varepsilon = 12\%$ each), 5 rings ($\varepsilon = 29\%$), flow obstructions pitch 100 mm.

$$\frac{\mathrm{CHF}_{\mathrm{enh\ tube}}}{\mathrm{CHF}_{\mathrm{ref\ tube}}} = 1 + R_{\mathrm{CHF}} = 1 + b\exp\left(-a\frac{L_{\mathrm{sp}}}{D}\right) \tag{1}$$

where R_{CHF} denotes the relative CHF enhancement, and is represented by either $R_{\mathrm{CHF,E}}$ for the entrainment-controlled region, or $R_{\mathrm{CHF,D}}$ for the deposition-controlled region.

In the entrainment-controlled region, the presence of flow obstacles in a flow channel enhances the CHF through (i) an increase in flow turbulence, which both increases the wall–liquid heat transfer and facilitates bubble detachment, and (ii) a change of phase distribution. Once turbulence is induced by an obstacle, the turbulence will travel downstream, and the intensity of the turbulence will decay. The decay function depends on how far the turbulence has traveled and how fast the turbulence weakens. Therefore, $R_{\mathrm{CHF,E}}$ can be written as

$$R_{\mathrm{CHF,E}} = \left[b_1\beta\frac{k_\varepsilon}{f} - b_2\varepsilon\frac{P_{\mathrm{oc}}}{P}(1-x_0)Re_{\mathrm{m0}}^{-n}\right]\exp\left(-b_3\frac{L_{\mathrm{sp}}}{D}\right) \tag{2}$$

where the first term in brackets represents the fraction contributed by an increase of flow turbulence, while the second term denotes the fraction caused by phase redistribution. In this equation, the obstacle-edge coefficient β varies from 1.0 for obstacles with abrupt leading edges, to 0.3 for obstacles with streamlined shapes, ε is the blockage ratio, and f is the friction factor for bare tubes, given by $f = 0.046Re_{\mathrm{f0}}^{-0.2}$, in which R_{f0} is defined below. (P_{oc}/P) is the ratio of the wetted perimeter contacted by obstacles (P_{oc}) to the total wetted perimeter of the flow channel (P). The homogeneous Reynolds number, R_{m0}, is based on the quality at the obstacle location, x_0, and is defined as $Re_{\mathrm{m0}} = GD/\mu_{\mathrm{m}}$, where $1/\mu_{\mathrm{m}} = (x_0/\mu_{\mathrm{g}}) + ((1-x_0)/\mu_{\mathrm{f}})$, μ_{m} is the homogeneous dynamic viscosity, and μ_{g} and μ_{f} are dynamic viscosities of the saturated vapor and liquid, respectively.

The local drag coefficient k_ε is evaluated using Voj equation [5], modified to

$$k_\varepsilon = \frac{\sqrt{\varepsilon}}{1-\varepsilon}\left[2.12 + \frac{10^4(1-\varepsilon)^2}{Re_{\mathrm{f0}}}\right] \tag{3}$$

where Re_{f0} refers to the liquid Reynolds number at the obstacle location, which is defined as

$$Re_{\mathrm{f0}} = \frac{GD}{\mu_{\mathrm{f}}}\left[(1-x_0) + \frac{\rho_{\mathrm{g}}}{\rho_{\mathrm{f}}}x_0\right].$$

The best-fit coefficients in Eq. (2) are $b_1 = 0.0048$, $b_2 = 2\times10^7$, $n = 1.25$ and $b_3 = 2.45\times Re_{\mathrm{f0}}^{-0.311}$.

In the deposition-controlled region, the flow regime is annular flow with a very thin liquid film ($\ll$1 mm) on the wall. Here, the primary mechanism of CHF enhancement is the increase in turbulence of the droplet-laden gas stream, which results in a significant increase in the

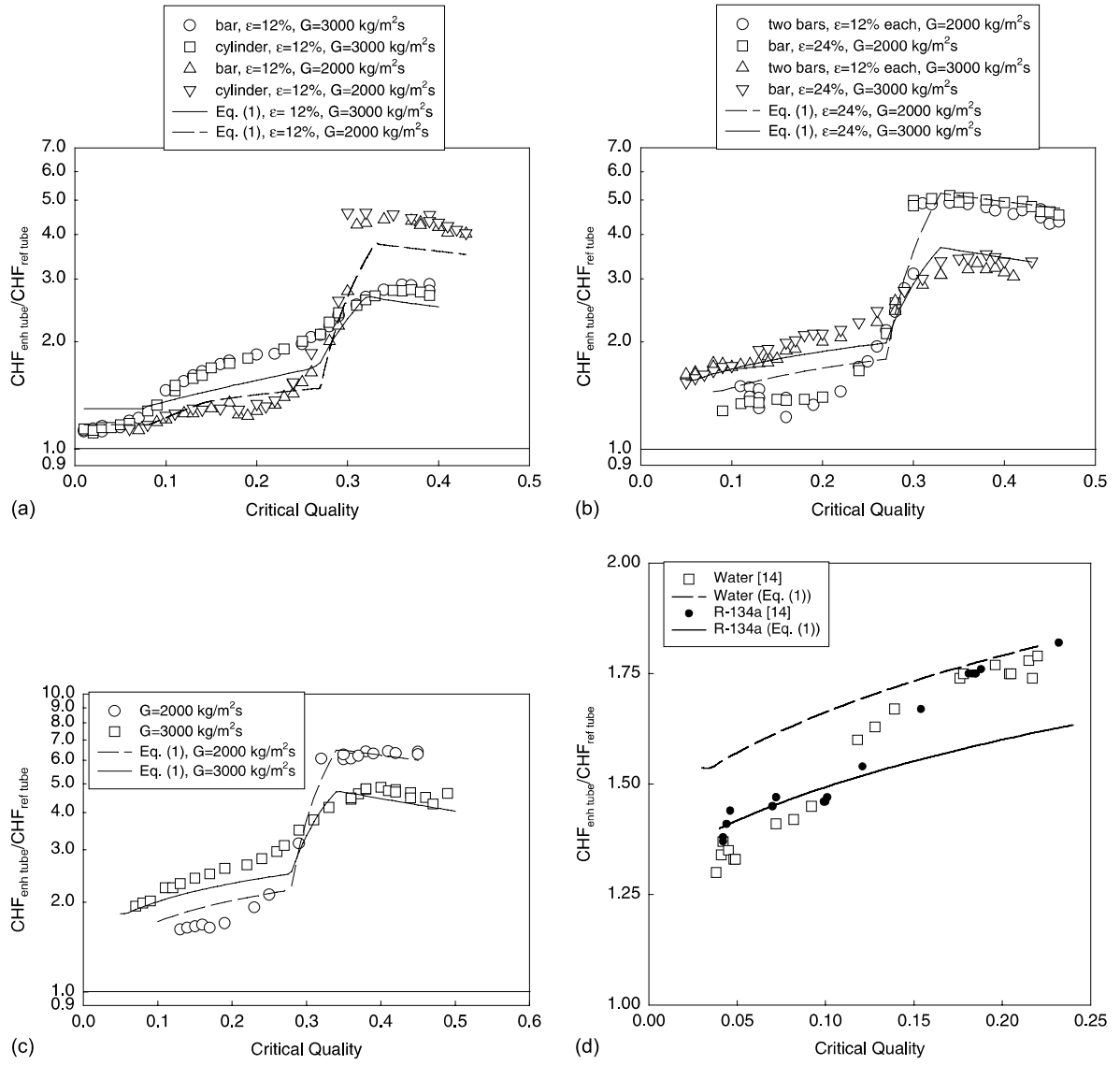

Fig. 16. Comparison of experimental data with prediction: R-134a, $p = 1.67$ MPa, (a) $\varepsilon = 12\%$ (bar, cylinder), (b) $\varepsilon = 24\%$ (bar, two bars), (c) $\varepsilon = 37\%$ (bar); (d) data [14], $D = 8$ mm, $L/D = 15.6$, $\varepsilon = 14\%$: water: $p = 10$ MPa, $G = 5500\ \mathrm{kg\,m^{-2}\,s^{-1}}$; R-134a: $p = 1.66$ MPa, $G = 3920\ \mathrm{kg\,m^{-2}\,s^{-1}}$.

deposition coefficient. The resulting CHF enhancement decays with distance downstream from the obstacle. In this study, a proportion of the CHF to the deposition rate was assumed. Hence, we have

$$R_{\mathrm{CHF,D}} = c_1 \frac{k_{\mathrm{D}\varepsilon} - k_{\mathrm{D}}}{k_{\mathrm{D}} Re_{\mathrm{v}}^{m}} \exp\left(-c_2 \frac{L_{\mathrm{sp}}}{D}\right) \tag{4}$$

where $k_{\mathrm{D}}\varepsilon$ and k_{D} are the deposition rates with obstacles and without obstacles, respectively. Windecker et al. [15] suggested that $k_{\mathrm{D}}\varepsilon = (1.4416\varepsilon + 1)k_{\mathrm{D}}$. Based on present experimental data, a smaller sensitivity of the relative CHF enhancement to the blockage ratio was found, and subsequently, Eq. (4) was modified to

$$R_{\mathrm{CHF,D}} = c_3 \varepsilon^{0.65} Re_{\mathrm{v}}^{-m} \exp\left(-c_2 \frac{L_{\mathrm{sp}}}{D}\right) \tag{5}$$

The new optimized coefficients are $c_3 = 1.9 \times 10^5$, $m = 0.67$ and $c_2 = 1.0 \times 10^{-6} Re_{\mathrm{m\,cr}}^{0.8}$, where $Re_{\mathrm{m\,cr}}$ is the homogeneous Reynolds number based on critical quality, and is defined as $Re_{\mathrm{m\,cr}} = GD/\mu_{\mathrm{m}}$, where $1/\mu_{\mathrm{m}} = (x_{\mathrm{cr}}/\mu_{\mathrm{g}}) + ((1 - x_{\mathrm{cr}})/\mu_{\mathrm{f}})$, μ_{m} is the homogeneous dynamic viscosity, and μ_{g} and μ_{f} are dynamic viscosities of the

saturated vapor and liquid, respectively; and Re_v is the vapor Reynolds number, defined as $Re_v = (GD/\mu_v)$.

The CHF enhancement ratio $CHF/CHF_0 = 1 + R_{CHF}$ can finally be predicted using Eqs. (1), (2) and (5), where R_{CHF} is either $R_{CHF,E}$ or $R_{CHF,D}$. In the transition between the entrainment-controlled and the deposition-controlled region, the CHF enhancement ratio is calculated by interpolation:

$$R_{CHF} = \begin{cases} R_{CHF,E} & \text{if } x_{cr} \leqslant 0.9x_{cr}^{lim} \\ \dfrac{x_{cr} - 0.9x_{cr}^{lim}}{0.2x_{cr}^{lim}}(R_{CHF,D} - R_{CHF,E}) + R_{CHF,D} & \text{if } 0.9x_{cr}^{lim} < x_{cr} < 1.1x_{cr}^{lim} \\ R_{CHF,D} & \text{if } x_{cr} \geqslant 1.1x_{cr}^{lim} \end{cases} \quad (6)$$

where x_{cr}^{lim} is the limiting critical quality given by Pioro et al. [10], and is expressed as

$$x_{cr}^{lim} = 1.0 - 0.86\exp(-19.0 \cdot We^{-0.5}) \quad (7)$$

where $We = (G^2D/\rho_f\sigma)$. If $x_{cr}^{lim} < 0.3$, then $x_{cr}^{lim} = 0.3$.

Comparisons of CHF enhancement predicted by Eq. (1) have been made using R-134a data from the University of Ottawa [7], R-134a and water data from Chalk River Laboratories [14] (Fig. 16). The present model is in reasonable agreement with R-134a data from the University of Ottawa, as well as R-134a and water data from Chalk River Laboratories [16]. The model slightly over-predicts the water CHF enhancement data (Fig. 16d). Compared to the existing CHF enhancement equations, the present model includes the effect of most of the important parameters (G, x_{cr}, ε, L_{sp}/D, shape and leading/trailing edge), and correctly represents the observed parametric and asymptotic trends [17].

5. Conclusions and final remarks

1. CHF experiments were performed in test sections with various types of flow obstacles and in a reference (bare) tube. The CHF enhancement results were compared with those of the reference tube, and with the CHF data from the look-up table.
2. The results show that the flow obstacles can have a significant enhancement effect on the CHF (up to 12 times, see Fig. 7a). The largest enhancement occurred for the largest flow blockage, and for qualities higher than the limiting critical quality for the reference tube.
3. The experiments showed that, at lower mass fluxes ($G \leqslant 1000\ kg\,m^{-2}\,s^{-1}$) and lower qualities ($x_{cr} < x_{cr}^{lim}$), the CHF enhancement effect of flow obstacles either disappears or becomes negative.
4. The effect of pressure on CHF enhancement is less clear. The least enhancement is generally encountered at the lowest pressure tested (6 MPa in water-equivalent value).
5. The distance from an upstream flow obstacle has a strong effect on CHF; the CHF enhancement decays exponentially with distance from the flow obstacle.
6. No limiting critical quality region was observed in the enhanced tube. It may well be that the turbulence generated by the obstacles destroyed the mechanisms that are responsible for the limiting critical quality.
7. The cross-sectional shape of the obstacle has a much smaller effect than the flow blockage ratio. For a given flow blockage ratio, flow obstacles that had a streamlined leading edge and those that blocked the liquid film flow (i.e., ring) were least effective.
8. Most of the above effects can be captured by the improved CHF enhancement prediction method presented in this paper.

Acknowledgements

The financial support provided by AECL and NSERC is gratefully acknowledged.

Appendix A. CHF and pressure drop in enhanced and reference tubes

Fig. 17 shows the effect of critical quality on the CHF enhancement ratio and the total pressure drop ratio, in

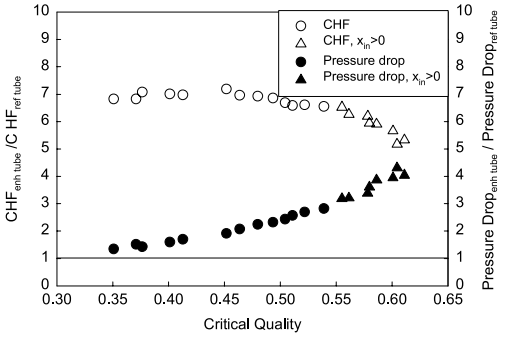

Fig. 17. Effect of critical quality on CHF enhancement and pressure drop ratios: R-134a, $p = 1.67$ MPa, $G = 2000\ kg\,m^{-2}\,s^{-1}$, $D = 6.92$ mm, $L = 1.92$ m; enhanced tube—one cylindrical obstacle ($\varepsilon = 37\%$) and 10 rings ($\varepsilon = 37\%$), flow obstructions pitch 100 mm.

the enhanced and reference tubes at flow boiling. The penalty for CHF enhancement in the tube equipped with flow obstructions at flow boiling is not so severe, compared with that in a single-phase flow. For a CHF enhancement ratio ranging from 7 to 5, the pressure drop ratio changes from 1.3 to 4.

References

[1] S.S. Doerffer, D.C. Groeneveld, J.R. Schenk, Experimental study of the effects of flow inserts on heat transfer and critical heat flux, Proceedings of the Fourth International Conference on Nuclear Engineering (ICONE-4), New Orleans, USA, March 10–14, 1996.

[2] S.S. Doerffer, D.C. Groeneveld, K.F. Rudzinski, et al., Some aspects of critical-heat-flux enhancement in tubes, Proceedings of the ASME International Mechanical Engineering Congress and Exposition (IMECE 2000), Orlando, Florida, USA, November 5–10, 2000, Paper 2-13-5-4.

[3] D.C. Groeneveld, K. Joober, S. Doerffer, et al., The effect of fuel subchannel geometry on CHF, Proceedings of the Fifth International Topical Meeting on Nuclear Reactor Thermal-Hydraulics (NURETH-5), Salt-Lake-City, Utah, USA, Vol. II, September 1992, pp. 683–690.

[4] D.C. Groeneveld, B.P. Kiameh, S.C. Cheng, Prediction of critical heat flux (CHF) for non-aqueous fluids in forced convective boiling, in: Proceedings of the Eighth International Heat Transfer Conference, vol. 5, 1986, pp. 2209–2214.

[5] D.C. Groeneveld, W.W. Yousef, Spacing devices for nuclear fuel bundles: a survey of their effect on CHF, post-CHF heat transfer and pressure drop, Proceedings of the ANS/ASME Topical Meeting on Nuclear Reactor Thermalhydraulics, Saratoga, NY, USA, October, 1980.

[6] I.L. Pioro, D.C. Groeneveld, S.C. Cheng, et al., Experimental study of the effect of flow obstructions in a circular tube on the critical heat flux, Proceedings of the Nineth International Topical Meeting on Nuclear Reactor Thermal-Hydraulics (NURETH-9), San Francisco, California, USA, October 3–8, 1999, Paper Log# 227.

[7] I.L. Pioro, D.C. Groeneveld, S.C. Cheng, et al., Effect of flow obstruction shape on the critical heat flux, Proceedings of the Eighth International Conference on Nuclear Engineering (ICONE 8), Baltimore, Maryland, USA, April 2–6, 2000, Paper 8350 (Track 7.04).

[8] I.L. Pioro, S.C. Cheng, A. Vasic, R. Felisari, Some problems for bundle CHF prediction based on CHF measurements in simple flow geometries, Nuclear Engineering and Design 201 (2–3) (2000) 189–207.

[9] I.L. Pioro, D.C. Groeneveld, S.C. Cheng, et al., Effect of flow obstacles with various leading and trailing edges on critical heat flux, Proceedings of the Nineth International Conference on Nuclear Engineering (ICONE-9), Nice, France, April 8–12, 2001, Paper #668.

[10] I.L. Pioro, S.C. Cheng, A. Vasic, I. Salah, Experimental evaluation of the limiting critical quality in circular and non-circular geometries, Nuclear Engineering and Design 190 (1999) 317–339.

[11] I.L. Pioro, D. Groeneveld, S.C. Cheng, et al., Comparison of CHF measurements in R-134a cooled tubes and the water CHF look-up table, International Journal of Heat and Mass Transfer 44 (1) (2001) 73–88.

[12] D.C. Groeneveld, L.K.H. Leung, P.L. Kirillov, et al., The 1995 look-up table for critical heat flux in tubes, Nuclear Engineering and Design 163 (1996) 1–23.

[13] S.C. Cheng, I.L. Pioro, S.S. Doerffer, et al., Critical heat flux for R-134a flow boiling in vertical tubes, in: Trends in Heat, Mass and Momentum Transfer, vol. 6, Research Trends, India, 2000, pp. 89–110.

[14] S.S. Doerffer, Private communications (2000).

[15] U. Windecker, Ch.Yu. Gu, J. Dennhardt, Droplet deposition in the annular flow regime with and without the influence of a spacer, Proceedings of the Nineth International Topical Meeting on Nuclear Reactor Thermal-Hydraulics (NURETH-9), San Francisco, California, USA, October 3–8, 1999, Paper Log #295.

[16] D.C. Groeneveld, I.L. Pioro, Y. Guo, et al., Experimental and analytical study of the effect of flow obstacles on the critical heat flux, in: Proceedings of the Fifth World Conference on Experimental Heat Transfer, Fluid Mechanics and Thermodynamics (ExHFT-5), Thessaloniki, Greece, vol. I, ETS Publishers, Pisa, Italy, September 24–28, 2001, pp. 251–258.

[17] Y. Guo, D.C. Groeneveld, S.C. Cheng, Prediction of CHF enhancement due to flow obstacles, International Journal of Heat and Mass Transfer 44 (2001) 4557–4561.